

# A Wideband Waveguide Diplexer for the Extend C-Band Antenna Systems

Jin Wang<sup>1, \*</sup>, Biao Du<sup>1, 2</sup>, Yang Wu<sup>2, 3</sup>, and Ying-Ran He<sup>1</sup>

**Abstract**—A wideband diplexer for the extended C-band feed antenna system is proposed in this paper. The diplexer operates in the receiving band (Rx) 3.625–4.8 GHz and transmitting band (Tx) 5.85–7.025 GHz, which give 28% and 19% bandwidths at Rx and Tx bands, respectively. In order to cover such a broadband, a side coupling T-shaped junction and a corrugated low-pass filter scheme are adopted. The T-shaped junction and the filter are designed separately, and then combined for optimization. A prototype is fabricated and measured. Measured results show a good agreement with the calculated ones. The return loss is less than  $-21$  dB, transmission loss less than 0.21 dB, Rx/Tx isolation better than 45 dB, and Tx/Rx isolation better than 70 dB.

## 1. INTRODUCTION

Recent developments in satellite communication antennas are related to dual-band antennas and integrated feed assembly technology offering low loss and dual polarization [1]. The capacity of antennas can be increased by simultaneously transmitting and receiving two pairs of signals on the same transmit and receive frequencies if the two pairs of transmit and receive signals are polarized [2]. For dual-band and dual-linear polarization antenna, one type of feed system is composed of two parts: wide-band orthomode transducer (OMT) and diplexer [3]. The diplexer is used for separating Rx and Tx linearly polarized signals.

Several diplexers were reported in the past [3–11]. A C-band diplexer is proposed in [3]. The relative frequency bandwidth of the diplexer is about 54%, and the transmitting and receiving bands have relative frequency bandwidths of 7% and 6.5%, respectively. The design is based on a waveguide *E*-plane bifurcation junction with a scattering element to satisfy the wideband common port matching. Several *H*-plane and *E*-plane T-shaped junctions are proposed in [4–7]. These designs are based on waveguide cavity filters realized with metal inserts or with irises and a common three-port waveguide junction. The overall bandwidth of such designs is restricted by dispersion effects and especially by higher order cavity modes. Suitable designs may cover an overall bandwidth up to 25%. Instead of using a T-shaped junction, Y-junction diplexers are presented in [8–10]. By using metal inserts in the vertical symmetry plane, the bandwidth is increased to 50%. Rosenberg et al. proposed a waveguide diplexer with ultra-broad band [11], operating in a 65% bandwidth (3.6–7.15 GHz). It is based on a common waveguide with dual-ridge cross section to ensure definite operation and interfacing solely with the TE<sub>10</sub> fundamental mode. Ridge waveguide band-pass filters are employed. The lower operating band is 3.6–4.2 GHz and the upper band 5.925–7.125 GHz, corresponding to 18% and 20% bandwidth, respectively.

This paper presents a wideband diplexer to meet the requirements in the extended C-band satellite communication, operating in 3.625–4.8 GHz (Rx) and 5.85–7.025 GHz (Tx), corresponding to 28% and

---

Received 31 August 2016, Accepted 24 October 2016, Scheduled 10 November 2016

\* Corresponding author: Jin Wang (15831969575@139.com).

<sup>1</sup> The 54th Research Institute of China Electronics Technology Group Corporation, Shijiazhuang, Hebei 050081, China. <sup>2</sup> Joint Laboratory for Radio Astronomy Technology, Shijiazhuang, Hebei 050081, China. <sup>3</sup> National Astronomical Observatories, Chinese Academy of Sciences, Beijing 100012, China.

19% bandwidths, respectively. The broadband performance is obtained by using a corrugated low-pass filter and a side coupling  $E$  plane T-shaped junction. This approach overcomes dispersion effects and higher order cavity modes by the combination of a corrugated low-pass filter and cutoff waveguide at high-pass port. The proposed diplexer is simulated, fabricated and measured. The measured results show a good agreement with the calculated ones. The return loss is less than  $-21$  dB, transmission loss less than  $0.21$  dB, Rx/Tx isolation better than  $45$  dB, and Tx/Rx isolation better than  $70$  dB. Measured results of our fabricated diplexer verify our design. Since the diplexer is compact and easily manufactured, it is very suitable for mass production.

## 2. CORRUGATED LOW-PASS FILTER DESIGN

Low-pass filters are extensively used in microwave systems for rejecting unwanted spectrum over broad frequency ranges. Broad pass-band, broad stop-band, low insertion loss and out-of-band rejection are the key requirements in satellite communication antenna feed systems. Most of the conventional diplexers are based on waveguide cavity filters realized with metal inserts or irises. The overall bandwidth of such designs is restricted by dispersion effects and especially by higher order cavity modes. For reducing spurious harmonics from transmitters, corrugated waveguide has been used as low pass filters in numerous feed systems [13–15].

Figure 1(a) shows the simulation model of the low-pass corrugated filter. The filter is an asymmetric structure, formed by  $N = 9$  corrugations in series and an impedance transformer. The coupling gap  $a = 11.8$  mm and all corrugations width  $b = 44.58$  mm will be constant. Port 1 is a rectangular waveguide of  $44.58$  mm  $\times$   $20.06$  mm. Port 2 is stepped to standard waveguide WR229. The other dimensions of the filter are regarded as parameters to be optimized, as illustrated in Figure 1(b) and Figure 1(c).

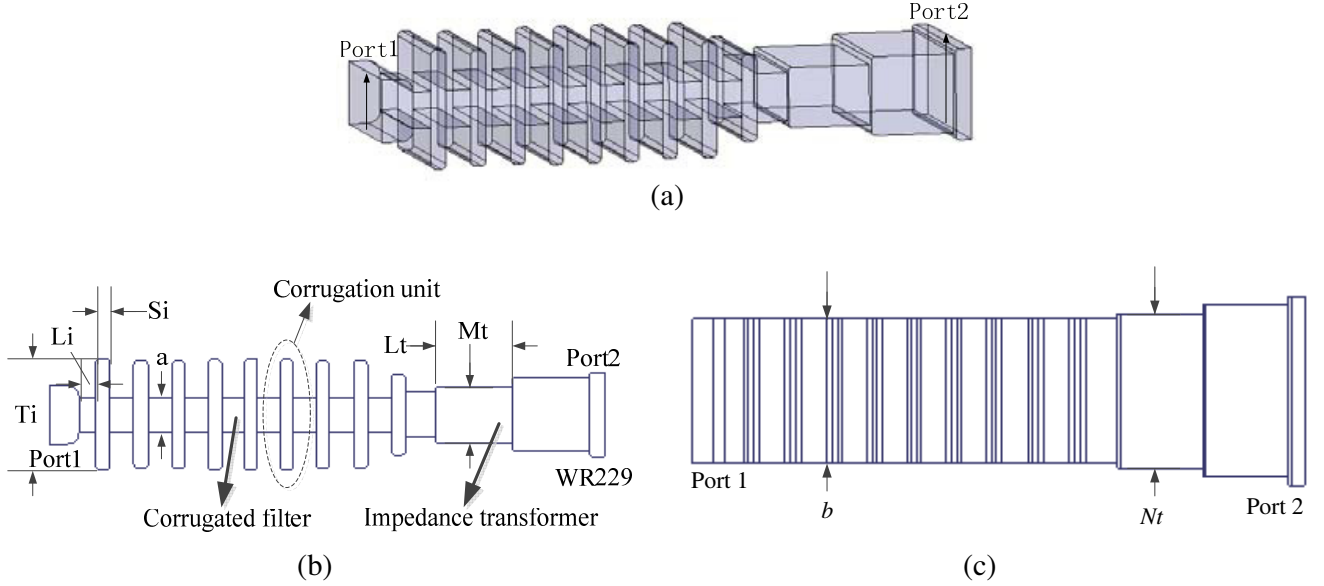


**Figure 1.** Geometry of the proposed corrugated filter. (a) 3D simulation model. (b) Side view of the corrugated filter, the corrugation width, height and the length between corrugation are  $S_i$ ,  $T_i$  and  $L_i$ , respectively, with  $i = 1, 2, \dots, 9$ ; the width and length of each transformer step are  $M_t$  and  $L_t$ , respectively, with  $t = 1, 2, 3$ . (c) Top view of the corrugated filter, the height of each transformer step is  $Nt$  with  $t = 1, 2, 3$ .

The corrugated filter may be designed for a prescribed stop band for the dominant  $TE_{10}$  mode, but also for the higher order  $TE_{n0}$  modes. The following expression is used to predict the spurious responses [13]

$$f_n = \sqrt{f_1^2 + (n^2 - 1) f_{c10}^2} \quad (1)$$

where  $f_n$  is the maximum frequency of the pass band of each  $TE_{n0}$  mode and  $f_{c10}$  the cutoff frequency of the  $TE_{10}$  mode.

This formula states that given a corrugated filter consisting of ideal cascaded transmission lines, the performance in a pure incident  $TE_{n0}$  mode at a frequency  $f_n$  is identical to that of the  $TE_{10}$  mode at the frequency  $f_1$ . Equation (1) predicts  $TE_{n0}$  propagation between frequencies  $nf_{c10}$  and  $f_{n0}$ , where  $f_{n0}$  is given by Eq. (1) with  $f_1 = f_{10}$ , the upper cutoff frequency of the filter to the  $TE_{10}$  mode.

Figure 2(a) depicts a corrugation unit formed by two step-junction discontinuities, and Figure 2(b) shows its equivalent network. According to [12], the corrugation unit of Figure 2(a) can be characterized by a cascade of  $S$ -matrices of two step-junctions. The expressions of the  $Y$ -matrix members can be obtained from [15].

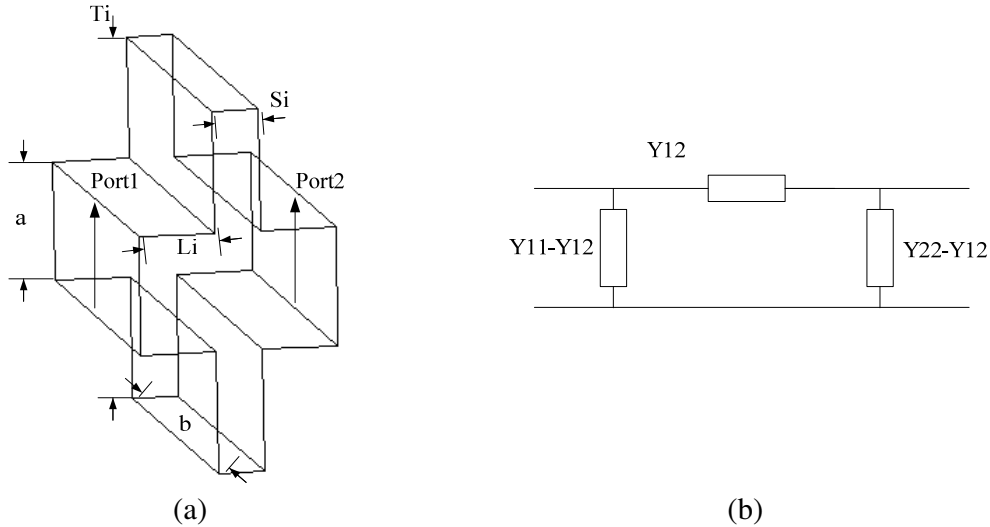


**Figure 2.** Structure of the proposed corrugation unit. (a) The 3-D view. (b) Equivalent network.

In order to analyze the effect of these parameters on  $S$ -parameters, a low-pass filter element of two corrugation units is investigated. The physical structure of the element is shown in Figure 3(a). When one parameter is studied, the others are kept constant.

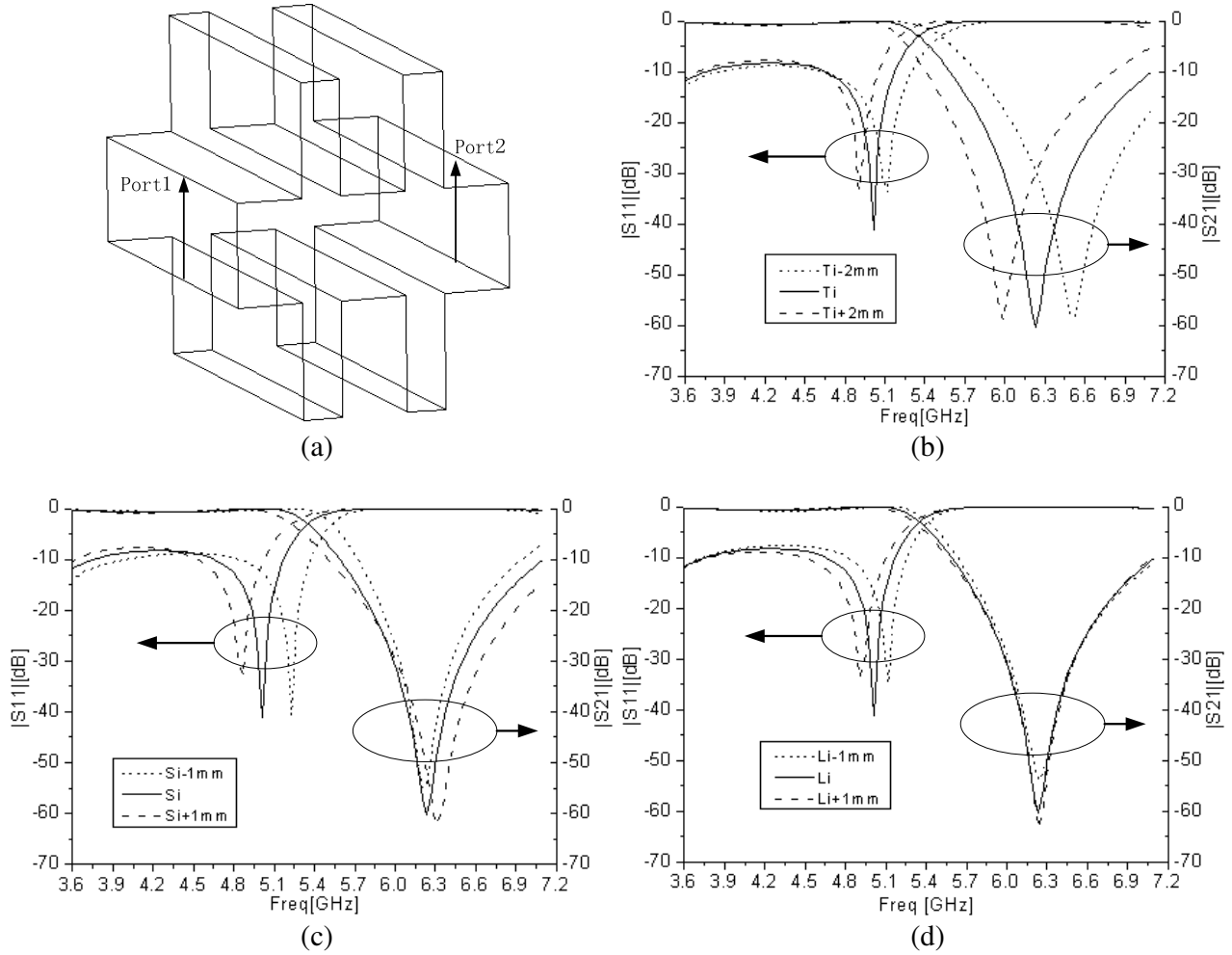
Figure 3(b) shows the effect of  $T_i$  on  $S$ -parameters. From Figure 3(b) it can be seen that when  $T_i$  increases, the pass-band impedance bandwidth becomes narrower, and the highest frequency point decreases slightly. The corrugation height mainly affects the specified frequency point of stop-band. When the  $T_i$  increases, the specified frequency point of stop-band decreases.

Figure 3(c) shows the effect of  $S_i$  on  $S$ -parameters. When  $S_i$  increases, the pass-band impedance bandwidth becomes narrower; the highest frequency point decreases; the specified frequency point of stop-band changes slightly. So it can be concluded that the corrugation width mainly affects the pass-band impedance bandwidth.

The effect of  $L_i$  is also analyzed as illustrated in Figure 3(d). When  $L_i$  decreases, the impedance bandwidth becomes narrower slightly, but the specified frequency point of stop-band is unchanged. So it can be concluded that the effects of this variation on filter performance are minor. Setting  $L_i$  to the minimum value can reduce the filter length.

Using the technique described in the previous paragraph, it is feasible to design the filter with required stop-band characteristics. However, matching networks must be still added at the input and output of the filter. As shown in Figure 1, an impedance transformer is employed to provide the device with standard waveguide port WR229, and matching was achieved by means of optimizing the corrugations and impedance transformer to obtain the required return loss.

The simulations and optimizations of the filter are carried out by commercial software  $\mu$ -wave. The calculated results are shown in Figure 4. The return loss is less than  $-25$  dB at Rx band, and the isolation is better than 75 dB at Tx band.



**Figure 3.** Geometry and simulated response of the filter using two corrugation units. (a) Geometry of low-pass filter unit using two corrugation units. (b) Simulated response with varying the corrugation height  $T_i$ ,  $T_i = 38\text{ mm}$ . (c) Simulated response with varying the corrugation width  $S_i$ ,  $S_i = 4.6\text{ mm}$ . (d) Simulated response with varying the length  $L_i$  between corrugation,  $L_i = 7.6\text{ mm}$ .

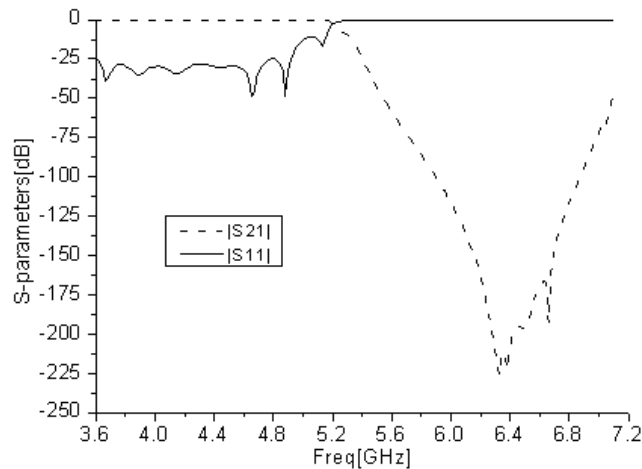


**Figure 4.** Simulated results of the proposed filter.

### 3. T JUNCTION DESIGN

The side coupling  $E$  plane T-shaped junction is shown in Figure 5(a) [16, 17], which passes through the Tx band signal, and the Rx band signal is cut off. In this procedure, we focus on the side branch which for the Tx band.

According to [12], in a rectangular waveguide of inner dimensions  $a$  and  $b$ , the cutoff wavelength for the  $TE_{mn}$ -mode is

$$\lambda_c = \frac{2\sqrt{ab}}{\sqrt{m^2\frac{b}{a} + n^2\frac{a}{b}}} \quad (2)$$

For rectangular waveguide filled with air, we assume  $a > b$ . The lowest cutoff frequency occurs for the  $TE_{10}$  ( $m = 1, n = 0$ ) mode, and the dominant mode of the rectangular waveguide:

$$f_{c10} = \frac{c}{2a} \quad (3)$$

where  $c$  is the speed of light in free space. At a given operating frequency  $f$ , only those modes having  $f > f_c$  will propagate.

In the T-shaped junction application, the side waveguide dimensions are chosen so that  $f_L = 4.8$  GHz is cut off, and  $f_H = 5.85$  GHz can still propagate. To obtain good performance, the longest

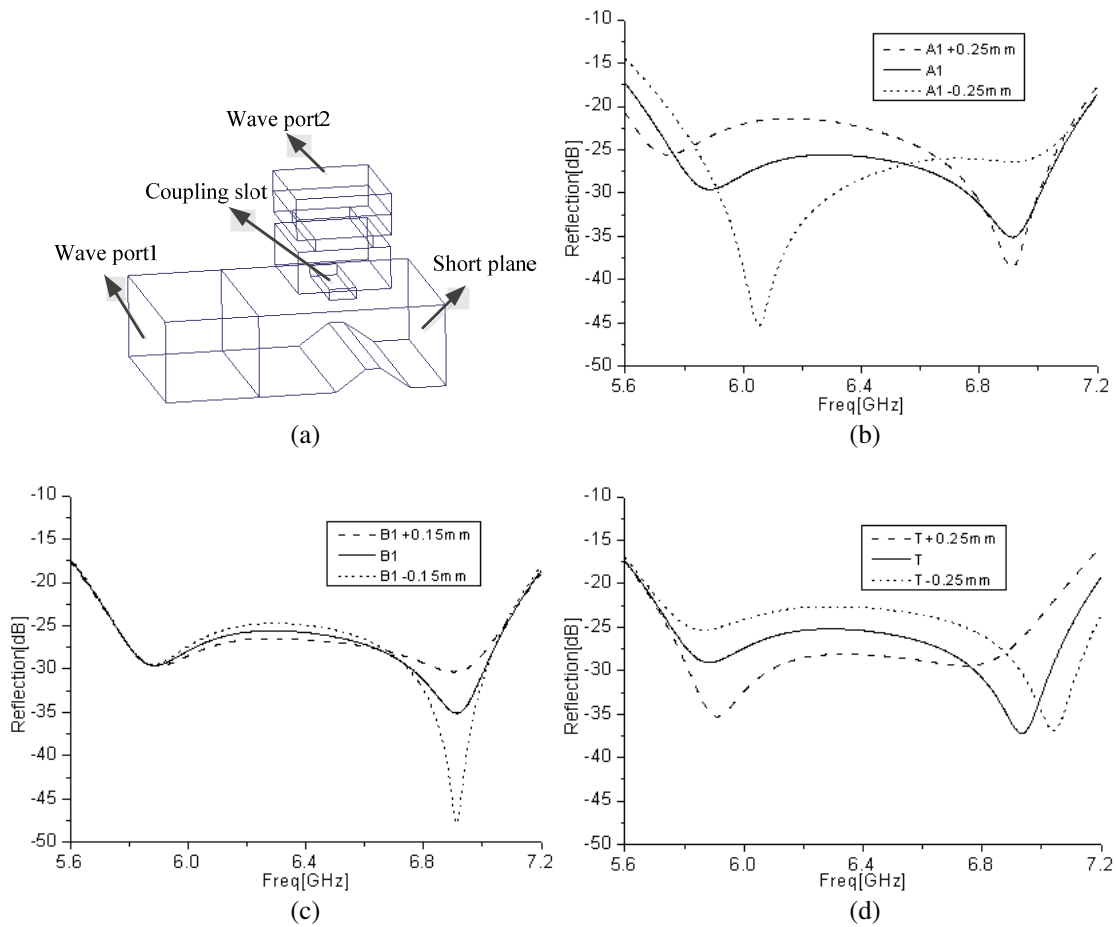


**Figure 5.** Geometry and simulated results of the T-shape junction. (a) Geometry of the T-shape junction. (b) Simulated response with varying length  $A1$  of the coupling slot. (c) Simulated response with varying width  $B1$  of the coupling slot. (d) Simulated response with varying distance  $T$  between the coupling slot and short plane.

side initial parameter of the side waveguide is chosen as the cutoff frequency  $f_M = 5.35$  GHz, and the corresponding dimension is 28 mm.

It is well known that the low-pass filter provides a short plane for the upper frequency band. Hence, in the T-shaped junction design, the Rx frequency band path is set to be a short plane, instead of a waveguide port. In this way, the calculation of the T-shaped junction can be carried out more quickly. The wave port 1 and the short plane of the T-shaped junction have the same dimensions as the corrugated filter  $44.58 \text{ mm} \times 20.06 \text{ mm}$ , thus the T-shaped junction can be easily connected with the filter. The most critical dimensions of the T-shaped junction is the distance  $T$  between coupling slot and short plane, coupling slot length  $A_1$  and width  $B_1$ . The effects of the critical parameters on the proposed T-shaped junction are analyzed for further study. When one parameter is studied, the others are kept constant.

The simulated plots of Figure 5(b) show the effect of changing coupling slot length  $A_1$  by 0.25 mm from the nominal value. From Figure 5(b) it can be seen that when length  $A_1$  increases, the impedance bandwidth becomes narrower the changes occur at the lower band edge are most significant. In the worst case, the return loss degrades by 4.6 dB at 6.15 GHz, to  $-21.4$  dB with a coupling slot length of  $+0.25$  mm from the nominal value.

The simulated plots of Figure 5(c) show the effect of changing the coupling slot width  $B_1$  by 0.15 mm from the nominal value. When  $B_1$  increases, the changes that occur at the upper resonant frequency are most significant. The reflection is still better than  $-25$  dB over the whole band. In the worst case, reflection value degrades by 0.5 dB at the mid-band, to  $-25.02$  dB with a coupling slot width of  $-0.15$  mm from the nominal value. So it can be concluded that the effect of this variation on T-shaped junction performance is minor.

The effect of distance  $T$  between the coupling slot and short plane is also analyzed. As illustrated in Figure 5(d), when  $T$  decreases, the bandwidth becomes wider, but the return loss degrades by 2.6 dB at the mid-band, to  $-22.7$  dB with a length  $T$  of  $-0.25$  from the nominal value. When  $T$  increases, the bandwidth becomes narrower; the most significant changes occur at the upper band; the reflection degrades by 11.9 dB at the upper band edge, to  $-22.6$  dB with a length  $T$  of  $+0.25$  from the nominal value. Therefore,  $T = 30.06$  mm is chosen to be the nominal value.

Then an impedance transformer to the WR159 waveguide is designed as shown in Figure 6(a). The main dimensions of the whole T-shaped junction are shown in Figure 6(b). The whole T-shaped junction is optimized by 3D full-wave software CST, and the simulation reflection is depicted in Figure 6(b).

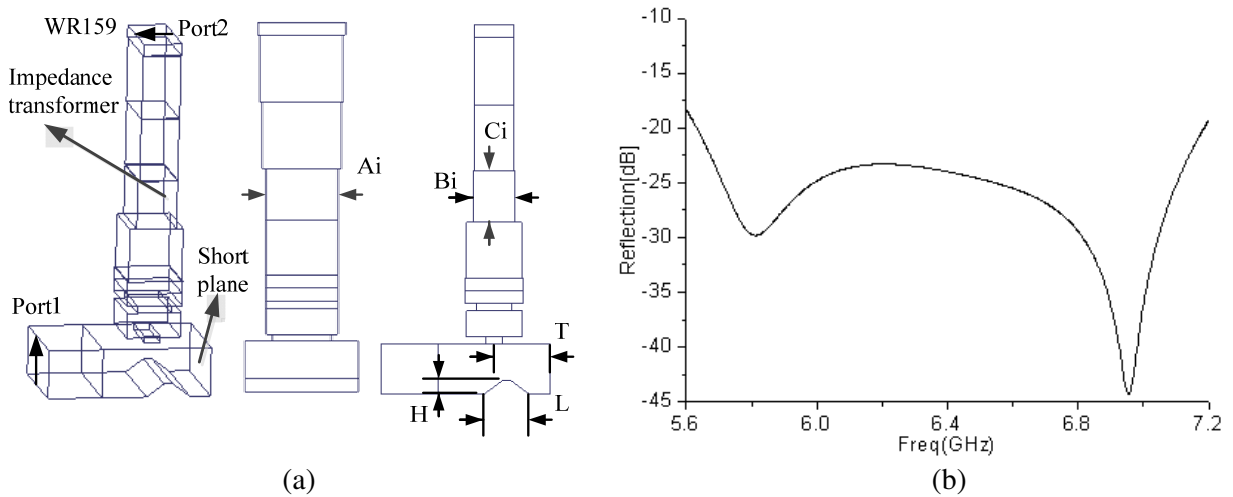


**Figure 6.** Geometry and simulated response of the T-shape junction including impedance transformer. (a) Geometry of the T-shape junction including impedance transformer, the length, width, and height of each step are  $A_i$ ,  $B_i$  and  $C_i$ , respectively, with  $i = 1, 2, \dots, 8$ . (b) Simulated reflection of the T-shape junction including impedance transformer.

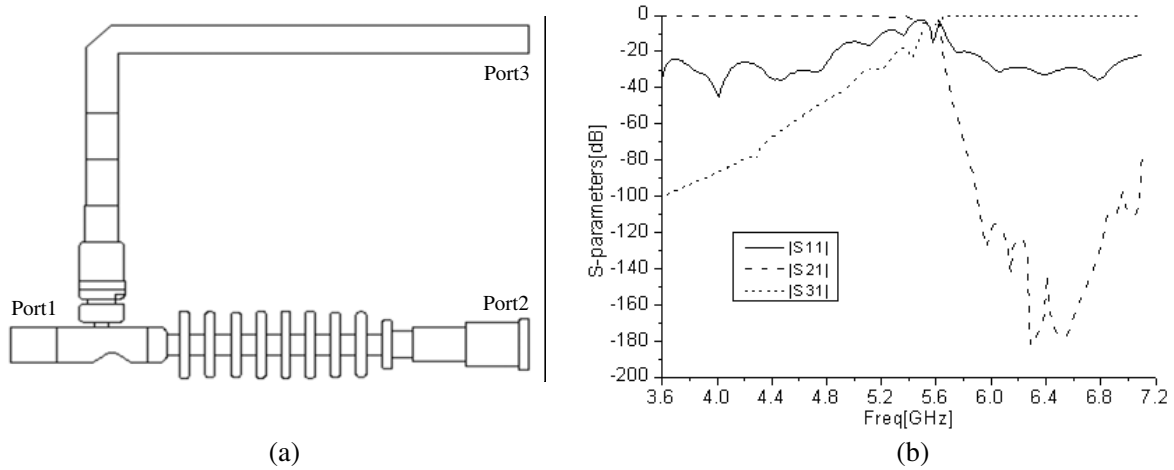


**Figure 7.** Geometry and simulated response of the proposed diplexer. (a) Side view of the whole diplexer configuration. (b) The simulated  $S$  parameters of the proposed diplexer.

**4. DIPLEXER DESIGN**

The filter and T-shaped junction designed in the previous sections are now connected to complete the diplexer design. The whole structure of the proposed diplexer is shown in Figure 7(a). Here port 2 is extended with an  $E$ -plane bend waveguide so that port 2 and port 3 are located in the same plane, which is useful for connection with receiving and transmitting modules.

The RF performance of the whole diplexer hardly ever achieves the wanted value, although the filter and T-shaped junction are well designed. This is mainly due to the variation of the short plane from the filter. Therefore, the whole diplexer needs to be re-optimized. The whole diplexer is optimized by using the commercial software  $\mu$ -wave. The simulated performance of the optimized diplexer is presented in Figure 7(b). The return loss is less than  $-23$  dB for both bands. The maximum insertion losses are 0.1 dB and 0.11 dB, for the Rx and Tx bands, respectively. The Rx/Tx isolation is better than 46 dB, and the Tx/Rx isolation is better than 95 dB. The parameters of the final diplexer design are listed in Table 1 to Table 3.

**Table 1.** Geometry dimensions of the corrugations.

$S_i$ (mm)	4.89	4.89	4.70	4.63	4.56	4.63	4.70	4.89	4.89
$T_i$ (mm)	38.08	37.01	36.81	37.95	37.95	37.95	36.81	37.01	27.69
$L_i$ (mm)	5.77	8.03	8.03	7.72	7.60	7.60	7.72	8.03	8.03

**Table 2.** Geometry dimensions of the filter impedance transformer.

$Mt$ (mm)	15.55	19.36	25.17
$Nt$ (mm)	44.58	47.33	52.94
$Lt$ (mm)	10.67	27.97	28.37

**Table 3.** Geometry dimensions of the T-shape junction.

$A_i$ (mm)	23.03	27.87	27.87	27.87	27.87	27.87	31.08	31.91
$B_i$ (mm)	6.44	22.37	13.88	22.87	22.12	16.51	15.80	15.80
$C_i$ (mm)	2.65	10.36	2.89	10.20	22.14	20.29	26.22	26.60
$H$ (mm)	5.31	$L$ (mm)	18.03	$T$ (mm)	32.54			

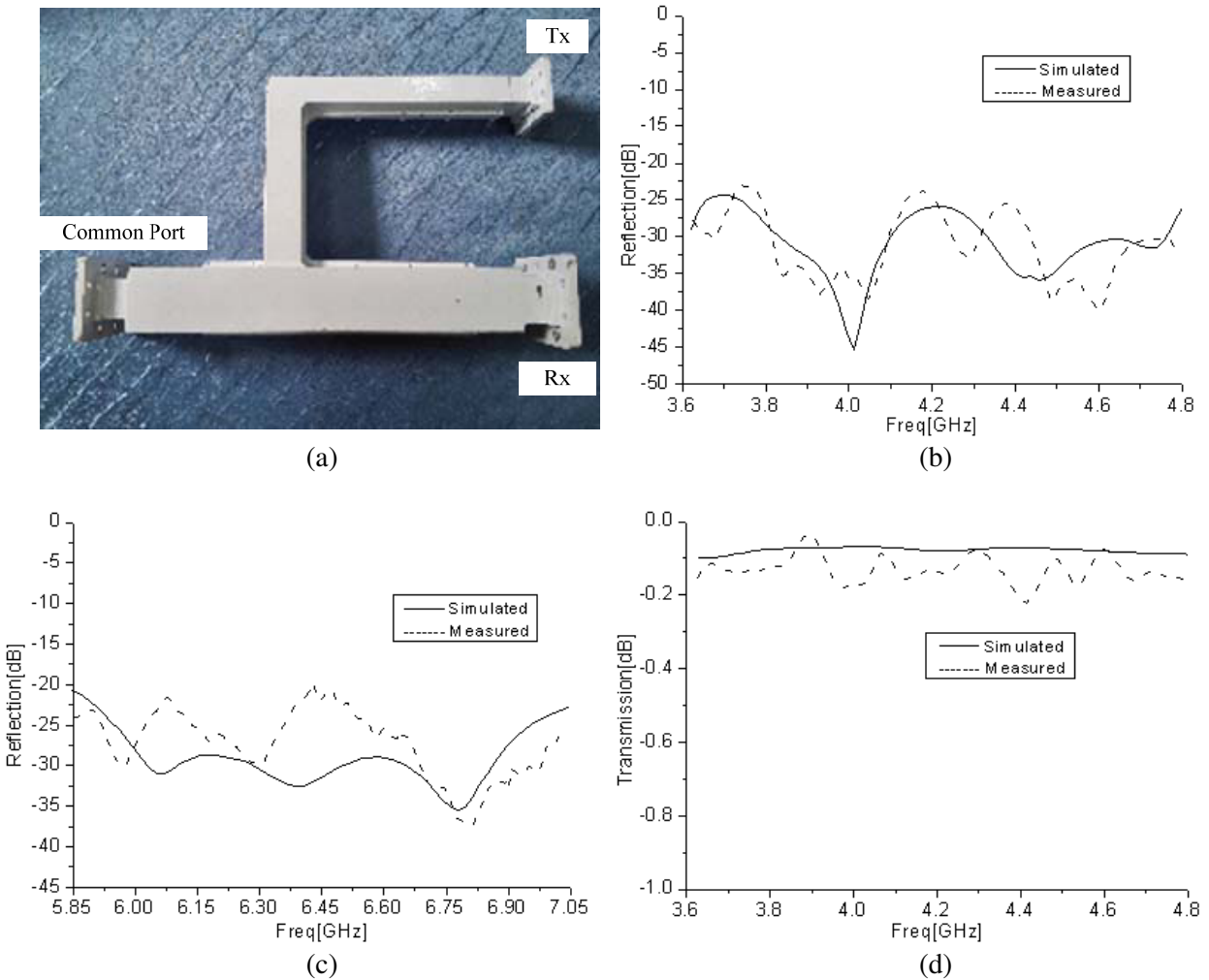
## 5. MEASURED RESULTS

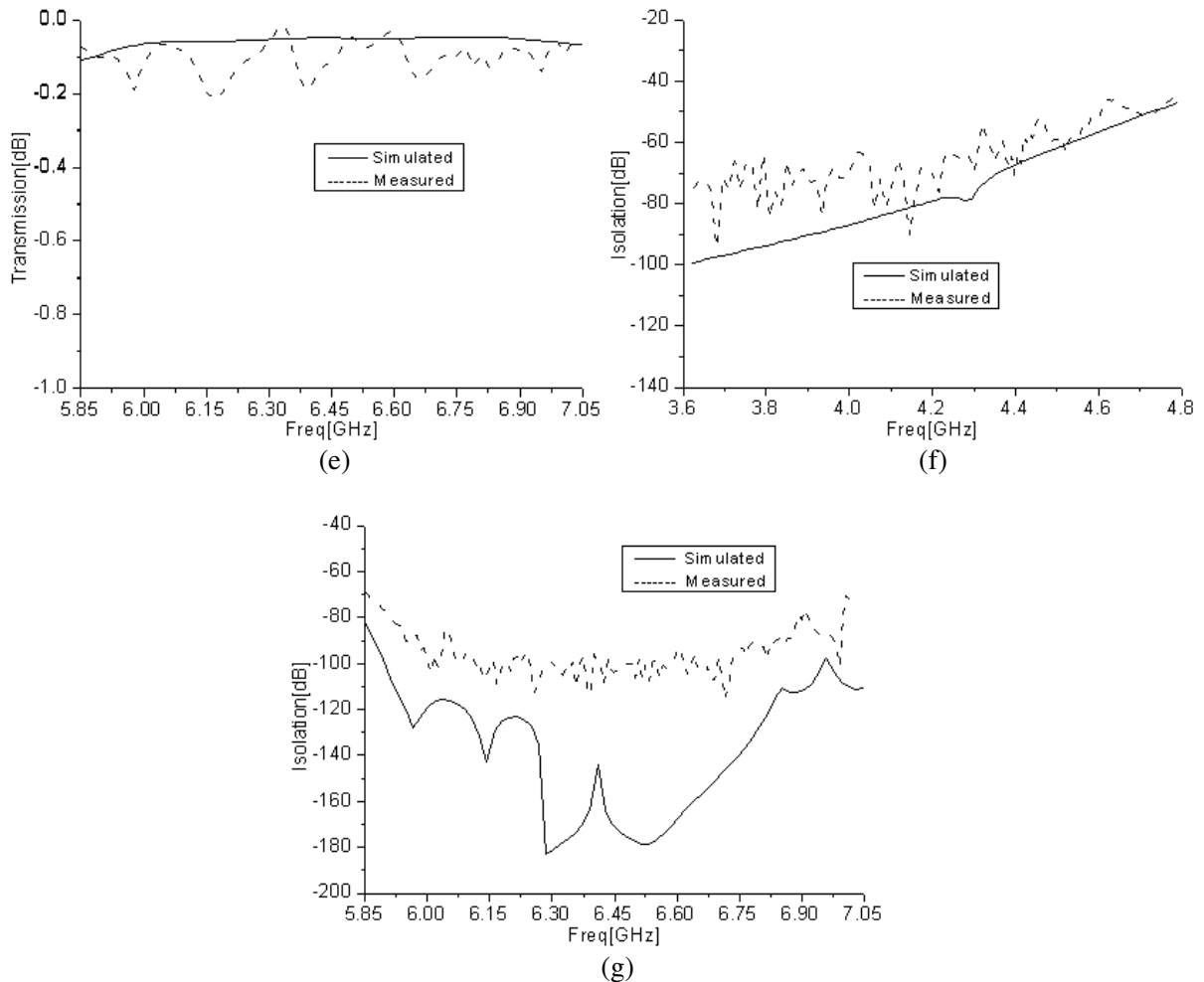
To verify the diplexer experimentally, a sample of the designed diplexer was fabricated, and its EM characteristics were measured. Figure 8(a) shows a photo of the manufactured diplexer.

Figure 8(b) and Figure 8(c) show simulated and measured diplexer reflections at the Rx and Tx bands. The measured response of Figure 8(b) shows a reflection of  $-23$  dB (at 3.76 GHz) or better across 3.625–4.8 GHz band, whereas the simulated response is  $-25$  dB (at 3.65 GHz) or better across the band. The measured response of Figure 8(c) shows a reflection of  $-21$  dB (at 6.45 GHz) or better across 5.85–7.025 GHz band, whereas the simulated response is  $-25$  dB (at 5.85 GHz) or better across the band. The simulated and measured results are correlated, with differences in response due mainly to the manufacturing tolerances of the fabricated device. The measured diplexer response exceeds our  $-20$  dB reflection specification.

Figure 8(d) and Figure 8(e) show simulated and measured diplexer insertion losses at the Rx and Tx bands. The measured insertion loss results are averaged from two diplexer units connected back to back. The measured response of Figure 8(d) shows that the insertion loss is less than 0.21 dB. The measured response of Figure 8(e) shows the insertion loss is less than 0.20 dB. The maximum simulated values are 0.1 dB and 0.11 dB, for the Rx and Tx bands, respectively. The simulated and measured results are compared. As expected, the measured insertion loss is higher than the ideal simulated values, with differences in response due mainly to the manufacturing tolerances of the fabricated device.

Figure 8(f) and Figure 8(g) show the simulated and measured Rx/Tx and Tx/Rx isolation between the two bands. The simulated isolation is very high due to the ideal geometry and mainly limited by





**Figure 8.** Manufacture and measured results of the proposed diplexer. (a) Photograph of the proposed diplexer. (b) Simulated and measured reflection coefficient at the Rx band. (c) Simulated and measured reflection coefficient at the Tx band. (d) Simulated and measured transmission coefficient for the Rx band. (e) Simulated and measured transmission coefficient for the Tx band. (f) Simulated and measured Rx/Tx isolation between the two bands. (g) Simulated and measured Tx/Rx isolation between the two bands.

the mesh symmetry of the finite element model. As expected, the measured isolation is lower than the simulated value due to manufacturing tolerances. The measured isolation is better than 70 dB across the band, which indicates a reasonably fabricated structure.

## 6. CONCLUSION

In this paper, an extended C-band wideband diplexer is designed. Using a corrugated low-pass filter and a side coupling  $E$  plane T-shaped junction. The bandwidth of the diplexer is greatly extended. The relative bandwidth of the whole diplexer is about 64%, and the Rx and Tx frequency bandwidths are 28% and 19%, respectively. The prototype of the diplexer is tested, and the experimental results are consistent with simulated ones. The Rx and Tx band return losses are less than  $-21$  dB. The transmission loss is less than 0.21 dB, the Rx/Tx isolation better than 45 dB and the Tx/Rx isolation better than 70 dB. The experiment results show that the RF performances of diplexer can meet the specification without the assistance of tuning screws. So this design can considerably enhance the efficiency of mass production and can be widely used in many wideband feed assemblies.

## ACKNOWLEDGMENT

This work is supported by the Applied Fundamental Research Project Key Research Programme of Hebei Province (No. 16960404D), China.

## REFERENCES

1. Rao, S. K., "Advanced antenna technologies for satellite communications Payloads," *IEEE Transactions on Antennas and Propagation*, Vol. 63, No. 4, 1205–1217, 2015.
2. Uher, J., J. Bohrnemann, and U. Rosenberg, *Waveguide Components for Antenna Feed Systems: Theory and CAD*, Artech House, 1993.
3. Ruiz-Cruz, J. A., J. R. Montejo-Garai, J. M. Rebollar, and J. M. Montero, "C-band orthomode transducer for compact and broadband antenna feeders," *Electronics Letters*, Vol. 45, No. 16, 813–814, 2009.
4. Shen, T., K. A. Zaki, and T. G. Dolan, "Rectangular waveguide diplexers with a circular waveguide common port," *IEEE Transactions on Microwave Theory and Techniques*, Vol. 51, No. 2, 578–582, 2003.
5. Cannone, G. and M. Oldoni, "High-yield E-band diplexer for fixed radio point-to-point equipment," *International Journal of RF and Microwave Computer-Aided Engineering*, Vol. 24, No. 4, 508–512, 2014.
6. Chen, C., L. Chen, and P. Zhao, "A waveguide diplexer based on E-plane T-junction," *2014 15th International Conference on IEEE Electronic Packaging Technology (ICEPT)*, 1390–1391, 2014.
7. Skaik, T. and M. Abu Hussain, "Design of diplexers for E-band communication system," *13th Mediterranean Microwave Symposium (MMS)*, Saida, Lebanon, 2013.
8. Vanin, F.-M., D. Schmitt, and R. Levy, "Dimensional synthesis for wide-band waveguide filters and diplexers," *IEEE Transactions on Microwave Theory and Techniques*, Vol. 52, No. 11, 2488–2495, 2004.
9. Vanin, F. M., F. Frezza, and D. Schmitt, "Computer-aided design of Y-junction waveguide diplexers," *Progress In Electromagnetics Research C*, Vol. 17, 203–218, 2010.
10. Gál, T., J. Ladvánszky, and F. Lénárt, "Improvement of waveguide diplexer components," *Asia-Pacific Microwave Conference Proceedings*, 28–30, 2013.
11. Rosenberg, U., A. Bradt, M. Perelshtein, and P. Bourbonnais, "Extreme broadband waveguide diplexer design for high performance antenna feed systems," *2010 European IEEE Microwave Conference (EuMC)*, 1249–1252, 2010.
12. Marcuvitz, N., *Waveguide Handbook*, The Institution of Electrical Engineering (IEE), London, UK, 1986.
13. Levy, R., "Tapered corrugated waveguide low-pass filters," *IEEE Transactions on Microwave Theory and Techniques*, Vol. 21, No. 5, 526–532, 1973.
14. Arregui, I., F. Teberio, I. Arnedo, A. Lujambio, M. Chudzik, D. Benito, T. Lopetegi, R. Jost, F.-J. Görtz, J. Gil, C. Vicente, B. Gimeno, V. E. Boria, D. Raboso, and M. A. G. Laso, "High-power low-pass harmonic filters with higher-order  $TE_{n0}$  and non- $TE_{n0}$  mode suppression: Design method and multipactor characterization," *IEEE Transactions on Microwave Theory and Techniques*, Vol. 61, No. 12, 4376–4386, 2013.
15. De Paolis, F., R. Goulouev, J. Zheng, and M. Yu, "CAD procedure for high-performance composite corrugated filters," *IEEE Transactions on Microwave Theory and Techniques*, Vol. 61, No. 9, 3216–3224, 2013.
16. Xing, Q. and Q.-X. Chu, "Ku band waveguide diplexer with side coupling," *IEEE Asia-Pacific Microwave Conference Proceedings*, Vol. 1, 1–2, 2005.
17. Carceller, C., P. Soto, V. E. Boria, M. Guglielmi, and J. Gil, "Design of compact wideband manifold-coupled multiplexers," *IEEE Transactions on Microwave Theory and Techniques*, Vol. 63, No. 10, 3398–3407, 2015.